245-GHz LNA, Mixer, and Subharmonic Receiver in SiGe Technology

Yanfei Mao, Klaus Schmalz, Johannes Borngräber, and John Christoph Scheytt

***Abstract*—A four-stage common-base (CB) 245-GHz low-noise amplifier (LNA) and a fourth subharmonic 245-GHz transconductance mixer are presented. An integrated subharmonic receiver for sensing applications in the 245-GHz industrial–scientific–medical band is proposed. The receiver consists of a single-ended CB LNA, a fourth transconductance subharmonic mixer, a 60-GHz push–push voltage-controlled oscillator with a 1/32 divider, and an IF amplifier. It is fabricated in an SiGe: C BiCMOS technology with f_T and $f_{\max}$ of 300 and 500 GHz, respectively. Its measured single-ended gain is 21 dB at 243 GHz with a tuning range of 12 GHz, and a noise figure of 33 dB. The input 1-dB compression point is -37 dBm. The receiver dissipates at 358 mW.**

***Index Terms*—Common-base (CB) low-noise amplifier (LNA), millimeter-wave circuits, subharmonic mixer (SHM), SiGe technology, subharmonic receiver, 245 GHz, voltage-controlled oscillator (VCO).**

I. Introduction

An industrial–scientific–medical (ISM) band at 245 GHz with 2-GHz bandwidth is available in Europe, which could be used for imaging radar for security applications, biomedical sensors for medical diagnostics [1], as well as millimeter-wave gas spectroscopy [2].

In [3], a fully differential 220-GHz integrated receiver front-end without a voltage-controlled oscillator (VCO) has been demonstrated in SiGe technology. Both the LNA and mixer are implemented with differential signaling. Although differential signaling is more robust to common-mode noise, it comes at the expense of higher power and more complicated local oscillator (LO) distributions. In order to reduce power dissipation, a single-ended receiver structure is chosen in this study. Hence, a single-ended LNA and subharmonic mixer (SHM) were studied and implemented. Finally, a single-ended receiver comprising of the single-ended LNA and SHM is proposed.

Various LNAs with different topologies, such as common emitter or cascode, are reported. In [4], using SiGe technology, a differential three-stage common emitter LNA at 60 GHz with 18-dB gain and 22-GHz 3-dB bandwidth is reported. In [5], a two-stage cascode SiGe LNA with 13.5-dB gain and a noise figure (NF) of 9.6 dB at 122 GHz is reported. In that study, the cascode configuration was chosen for its high gain, high isolation, and wide bandwidth. In [3], a differential three-stage cascode LNA at 220 GHz with 15 dB is reported. This paper investigates a common-base (CB) topology and presents a four-stage LNA with high gain and low NF. Simulations and measurements show that CB LNAs are very sensitive to even a low parasitic inductance at the grounded base node. This effect is theoretically investigated.

TABLE I
Performance Comparison of SHMs

	RF/ft/fmax	Order subharmonic	Conv. Gain dB	NF dB
[1]	122	2^{nd}	21	21
[6]	77	2^{nd}	0.7	23
[7]	650	4^{th}	-13	42
[8]	60	4^{th}	-13.2	-

With respect to mixer design, SHMs offer an alternative solution to fundamental mixers in the millimeter-wave range since they allow for an LO at lower frequency [1]. In [1], a second SHM based on two stacked switching quads with conversion gain of 21 dB at 122 GHz and NF of 21 dB is reported. In [6], second transconductance subharmonic balanced mixers with 0.7-dB conversion gain at 77 GHz are demonstrated. In [7], a fourth transconductance SHM at 650 GHz with -13-dB conversion gain and 42-dB NF is presented. In [8], a fourth passive GaAs monolithic SHM with a maximum conversion loss of 13.2 d dB is achieved at 60 GHz. Table I gives a brief comparison between those different SHMs.

Comparing SHMs based on switching cores with transconductance SHMs, switching cores do not behave like switches at frequencies near the f_T of the transistsors while transconductance SHMs still function well even for frequencies beyond f_T (or $f_{\max}$) [7]. A comparison of the transconductance SHM with a passive SHM shows that the transconductance SHM has a better gain performance. Based on these considerations, a transconductance SHM topology is preferable. A fourth SHM was implemented, which can be used with an existing 60-GHz VCO.

Using an LNA, fourth SHM, and 60-GHz VCO, a single-ended 245-GHz receiver was implemented and measured. This paper is organized as follows. In Section II, semiconductor technologies for the different fabrication runs are briefly described. In Section III, the design of the CB LNA is presented together with a mathematical analysis of the influence of small parasitic

Manuscript received February 28, 2012; revised June 22, 2012; accepted July 03, 2012. Date of publication August 06, 2012; date of current version December 13, 2012. This work was supported by EFRE, Land Brandenburg under Project Tele-Diagnostik. This paper is an extended paper from the 12th IEEE Topical Meeting on Silicon Monolithic Integrated Circuits in RF Systems, Santa Clara, CA, January 16–18, 2012.

Y. Mao, K. Schmalz, and J. Borngräber are with IHP GmbH, D-15236 Frankfurt (Oder), Germany (e-mail: mao@ihp-microelectronics.com).

J. C. Scheytt was with IHP GmbH, D-15236 Frankfurt (Oder), Germany. He is now with the Department of System and Circuit Technology, University of Paderborn, Paderborn 33102, Germany.

Color versions of one or more of the figures in this paper are available online at http://ieeexplore.ieee.org.

Digital Object Identifier 10.1109/TMTT.2012.2209447

ground inductance. The SHM and the 60-GHz VCO are then presented. In Section IV, simulation and measurement results of the components and the integrated receiver are shown. This is followed by Section V in which different receiver topologies are discussed and an improved receiver topology is proposed. Finally, conclusions are given in Section VI.

II. Technology

We used three subsequent fabrication runs (run1, run2, and run3) for the fabrication of the receiver and its standalone subcircuits, LNA, SHM, VCO, and LNA-SHM chain. In the three runs, a different IHP GmbH semiconductor was utilized.

In run1, a four-stage CB 245-GHz LNA was designed in an experimental 0.25-μm BiCMOS (DotFive) technology. The technology has five metal layers. The five metal layers include three aluminum metal layers and two top-metal layers with 2- and 3-μm thickness, respectively. Low-loss transmission lines could be designed with the two thick top-metal layers. f_T and $f_{\max}$ of the experimental transistors are reported to be 300 and 500 GHz, respectively [14].

In run2, a fourth transconductance SHM was designed in IHP GmbH's standard 0.13-μm BiCMOS technology (SG13S). The CB LNA from run1 was also redesigned in this technology. The SG13S technology has seven aluminum layers. The seven layers include five thin metal layers and two top-metal layers with 2- and 3-μm thickness, respectively. The f_T and $f_{\max}$ of the transistors are 250 and 300 GHz, respectively [15].

In run3, a standalone LNA, a fourth transconducatance SHM, an LNA-SHM chain, and an LNA-SHM chain with a VCO were designed in an improved 0.13-μm BiCMOS technology (SG13G2). The technology has the same metal layers as that in run2 (SG13S), but with different transistors. The f_T and $f_{\max}$ of the transistor are 300 and 500 GHz, respectively [9].

III. Circuit Design

A GoldenGate RF integrated circuit simulator is utilized to design and optimize the receiver. Transmission lines were simulated with Momentum, and the simulation results were fitted to a transmission-line model TLINP in ADS. TLINP was then utilized in the circuit simulation. Inductors and transformers were simulated with 2.5-D planar electromagnetic (EM) simulator (Momentum), and S-parameters were obtained and utilized in circuit simulation.

The topology of the receiver is shown in Fig. 1. The receiver consists of a 245-GHz CB LNA, a fourth transconductance SHM, an IF amplifier (IFAMP), a 60-GHz push–push VCO, and a 1/32 frequency divider (FD) for the 30-GHz fundamental frequency output of the VCO. Conjugate matching is implemented between the LNA and mixer interface for maximum power transfer, and the VCO output is coupled to the SHM by a transformer.

The LNA, SHM, and VCO were designed and tested both as separate components, as well as in their fully integrated configurations as receivers. Besides standalone subcircuits, the LNA-SHM chain without a VCO is also designed and measured.

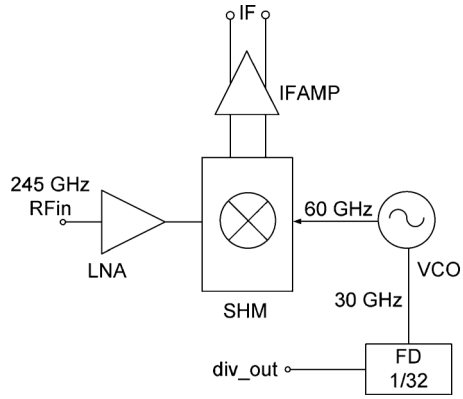

Fig. 1. Topology of the receiver.

In the following sections, the details of these circuit designs and the complete receiver design are presented.

A. CB Low-Noise Amplifier

A CB topology is chosen for each stage for its wide bandwidth, high gain, and high isolation at the operating frequency. The CB topology has a much better gain performance per stage than the common emitter topology. When comparing a two-stage CB with a cascode topology, it can be shown that due to the influence of the parasitic inductance between the base terminal and the ground, a CB stage can achieve comparable gain with lower power [10].

Fig. 2 shows the schematic of one stage of the four-stage CB LNA. Bond pad capacitances are included in both the input and output matching networks. In run1, $V_{\rm cb}$ provides the base bias for the CB transistor through resistor ladder R1 and R2. In run3, the bias circuit is modified, as shown in Fig. 2. Diode-connected transistor biasing is adopted in run3 in order to realize more accurate bias. Measurement results illustrating the improvement will be shown in Section IV. Transistor Q0 is biased at close to peak f_T collector current density in order to achieve high speed for Q0. $\rm TL_{sh}$ provide the dc ground for the emitters of the transistors, and with the $\rm TL_{ser}$ and metal–insulator–metal (MIM) capacitors C_n $(n = 1-4)$, form the input and inter-stage impedance matching network, where n presents the number of the stage in the four-stage CB LNA. Transmission lines $\rm TL_{load}$ represent inductive loads for each CB stage. $C_{\rm byp}$ provides the ac ground for the base connection and the dc supply.

For frequencies as high as 245 GHz, minor parasitics like pieces of short interconnects, the terminal connections, parasitic bottom capacitor of the MIM capacitor, etc., will affect the performance of the LNA. A parasitic inductance is utilized in this work to boost the gain of the LNA. The inductance may be caused by the connection between base terminal and bypass capacitor (ac ground) or the nonideal metal 1 ground plane and is in the range of 1–5 pH. At such high frequency, 245 GHz , this inductance has a strong influence on the LNA stability.

Fig. 3 shows a small-signal equivalent circuit of one stage of the CB LNA where L_B denotes the parasitic inductance between base terminal (B) and ac ground. The relevant transistor parasitics at high frequencies are r_B, C_π, C_μ, and C_S representing base resistance, base–emitter capacitance,

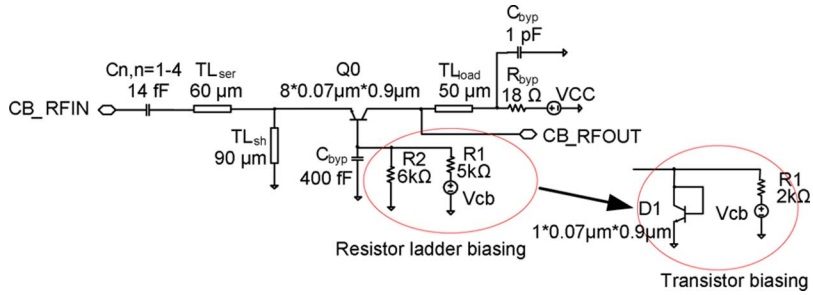

Fig. 2. Schematic of the one stage of the CB LNA.

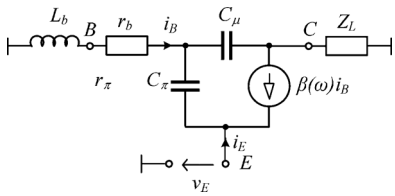

Fig. 3. Small-signal equivalent circuit of one stage of the CB LNA.

base–collector capacitance, and collector–substrate capacitance, respectively. In Fig. 3 C_S is included in the load impedance Z_L.

An analysis of the effect of the small parasitic inductance on the CB amplifier stability is given in the following. Since we are mostly interested in the influence of parasitics on the base side of the CB stage and in order to simplify the calculations, we neglect C_μ in the analysis. In (1), we define the complex input impedance Z_E at the emitter node. In (2), the current i_E is calculated. Applying Kirchhoff's voltage law to the base–emitter loop, we obtain (3). Rearranging (3) yields (4). Inserting (4) and (2) into (1) yields (5) as follows:

$$Z_E = \frac{v_E}{i_E} \tag{1}$$

$$i_E = -i_B(1+\beta(\omega)) \tag{2}$$

$$j\omega L_B i_B + r_B i_B + \frac{i_B}{j\omega C_\pi} + v_E = 0 \tag{3}$$

$$v_E = -i_B\left(j\omega L_B + r_B + \frac{1}{j\omega C_\pi}\right) \tag{4}$$

$$Z_E = \frac{\left(j\omega L_B + r_B + \frac{1}{j\omega C_\pi}\right)}{(1+\beta(\omega))}. \tag{5}$$

For angular frequencies $\omega > \omega_T/\beta_0$, we can approximate $\beta(\omega)$ by $\beta \approx -j\omega_T/\omega$. Using this approximation and (5), we obtain

$$Z_E \approx \frac{\left(j\omega L_B + r_B + \frac{1}{j\omega C_\pi}\right)}{\left(\frac{1-j\omega T}{\omega}\right)}. \tag{6}$$

From (6), we can calculate the real part of Z_E, which yields

$$Re\{Z_E\} \approx \frac{\left(r_B + \frac{\omega_T}{\omega^2 C_\pi} - \omega_T L_B\right)}{\left(1+\left(\frac{\omega T}{\omega}\right)^2\right)}. \tag{7}$$

From (7), we can see that the parasitic inductance L_B indeed may cause a negative real part of Z_E, i.e., a potential oscillation of the amplifier. In fact, the real part of Z_E becomes negative when the relation (8) is fulfilled as follows:

$$\frac{r_B}{\omega_T} + \frac{1}{\omega^2 C_\pi} < L_B. \tag{8}$$

From (8), it can also be seen that the tolerable parasitic inductance becomes smaller at high frequencies and can be increased by reducing ω_T. This can be achieved by reducing the dc collector current, and hence, the transconductance g_m. The collector current is determined by the base–emitter bias $V_{\rm be}$. Thus, by reducing base–emitter bias voltage $V_{\rm be}$, the negative resistance seen at the emitter can be reduced. In this way, the stability of the LNA is improved while reducing at the same time the amplifier gain. On the other hand, this property of the CB amplifier can be used deliberately to increase the CB amplifier gain to some extend.

More discussion about the impact of the parasitic inductance on the LNA performance is given in Section IV-A.

B. SHM

We chose transconductance mixing as the topology for the SHM. The reasons are well explained in [12]. In transconductance mixing, the time-varying transconductance is the dominant contributor to frequency conversion. The LO is a large signal and its voltage across the base and emitter junctions create a time-varying transconductance $G_m(t)$ [6]. In general, $G_m(t)$ is periodic, but not a sinusoidal signal, and can be represented as a Fourier series

$$G_m(t) = G_{m0} + G_{m1}\cos(\omega_{\rm LO}t) + G_{m2}\cos(2\omega_{\rm LO}t) + G_{m3}\cos(3\omega_{\rm LO}t) + \cdots.$$

The collector current i_C is the product of the $G_m(t)$ and input voltage $V_{\rm BIAS} + V_{\rm RF}\cos(\omega_{\rm RF}t)$. The output current consists of many mixing products. $(G_{m1}V_{\rm RF})/2\cos\left[(\omega_{\rm RF}-\omega_{\rm LO})\,t\right]$ is the fundamental mixing term, which could be utilized as fundamental frequency translation. In this paper, it is the $(G_{m4}V_{\rm RF})/2\cos\left[(\omega_{\rm RF}-4\omega_{\rm LO})\,t\right]$ term that generates the desired subharmonic mixing product and should be maximized for higher conversion gain. In principle, the fourth harmonic signal is a function of conduction duty cycle and its optimum value can be obtained when the transistor is biased close to its turn-on point.

The schematic of the 245-GHz subharmonic balanced mixer is shown in Fig. 4. Q1 and Q2 is the mixer core and they are biased close to the turn-on voltage in order to maximize the nonlinearity characteristic of the transistors. Resistor ladders are

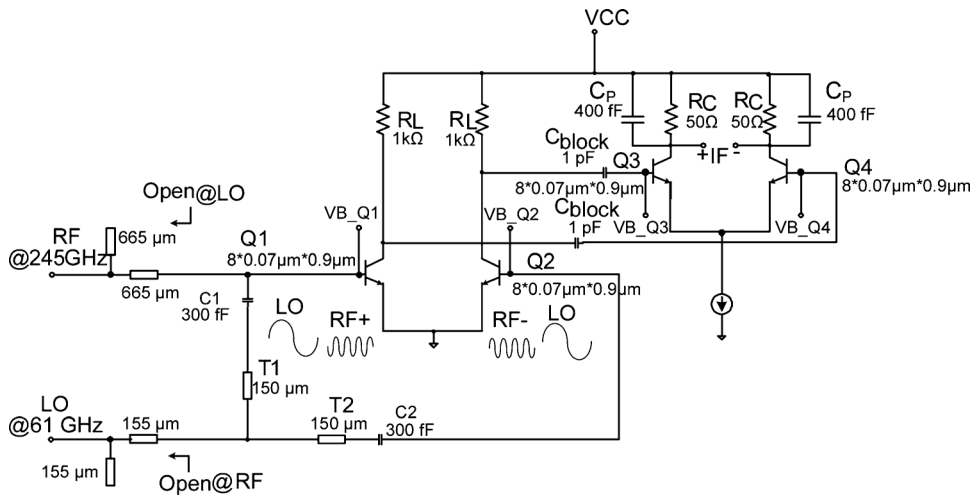

Fig. 4. Schematic of the one stage of fourth SHM.

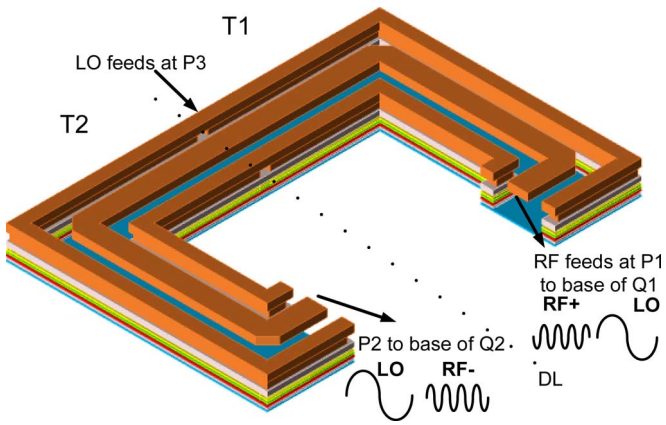

Fig. 5. Layout of T1, T2 and LO, RF signals feeding.

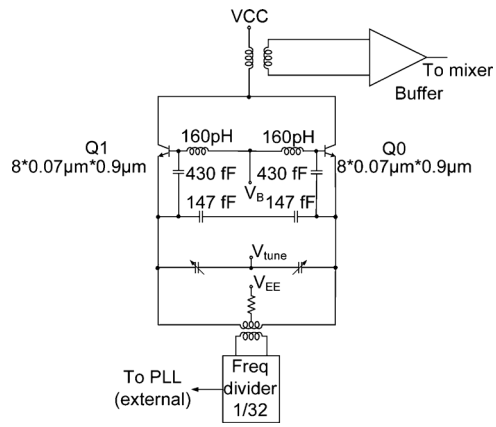

Fig. 6. Schematic of the push–push oscillator with buffer .

utilized for the Q1 and Q2 biasing. Two parallel shunt-series stub transmission lines are used to achieve isolation between the LO and RF ports. A quarter-wavelength at the LO open shunt stub and a quarter-wavelength at the LO series stub form an open impedance at the LO frequency. A quarter-wavelength at the RF open shunt stub and a quarter-wavelength at the RF series stub form an open impedance at the RF frequency. The two transmission lines T1 and T2 are used to provide 90° phase delay at 245 GHz and the whole input network makes the RF signals become out of phase, while the LO signals are kept in phase at the input of the transistors. In Fig. 5, layout of T1 and T2 are illustrated. The transmission line on the right of the dotted line DL is T1, the transmission line on the left of DL is T2. $\mathrm{RF}+$ feeds at P1. P1 is connected to the base of Q1, and port P2 is connected to the base of Q2. The $\mathrm{RF}+$ signal becomes $\mathrm{RF}-$ at P2 after it travels through T1 and T2. $\mathrm{RF}-$ is out of phase compared with $\mathrm{RF}+$. The LO signal feeds at port P3, and exhibit in-phase signals after traveling the same length of transmission lines T1 and T2, respectively.

In order to enable standalone SHM measurement, after the mixing core stage, a differential common emitter buffer stage is utilized as the output buffer stage to provide impedance matching to 50 Ω. 50-Ω resistive loads are used in the buffer for output matching. Filtering capacitors C_P (400 fF) are used parallel to the resistor loads to filter out frequency components higher than IF. Q3 and Q4 are biased with transistor biasing at the base terminal. This standalone SHM is used as well in the LNA-SHM-VCO integrated receiver. A capacitor of 1 pF is placed between the mixer and buffer stage for dc blocking.

In Fig. 1, an IFAMP follows the SHM. The IFAMP is a two-stage pseudo-differential common emitter amplifier. The IFAMP utilizes a 300-Ω resistor as the load.

C. VCO

The oscillator has to provide a 60-GHz single-ended signal to the fourth transconductance SHM. To fulfill all requirements in terms of tuning range, power, and reliability, a push–push oscillator topology was chosen. With this topology, it is possible to provide a signal path with relatively low fundamental frequency f_0 of 30 GHz to the FD and to provide the 60-GHz signal via a buffer to the fourth transconductance SHM.

The schematic of the push–push oscillator with a buffer is shown in Fig. 6. Buffer stages are CB circuits with the advantage of high gain at 60 GHz and robustness with respect to the supply voltage. A balun is connected to the single-ended LO power input for the fourth SHM.

The oscillator in this study has the same topology as the oscillator in [1], but was transferred to the IHP GmbH 0.13-μm SG13G2 BiCMOS technology.

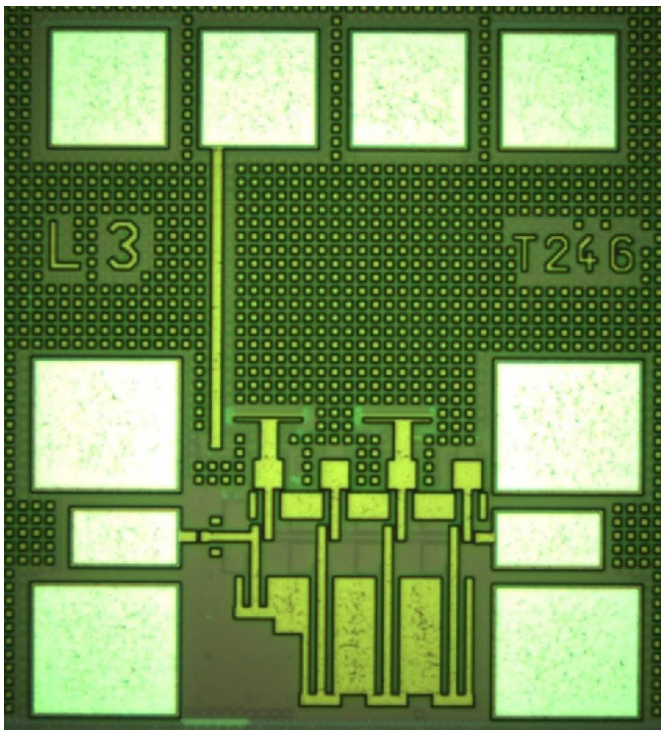

Fig. 7. Chip photograph of CB LNA, run1.

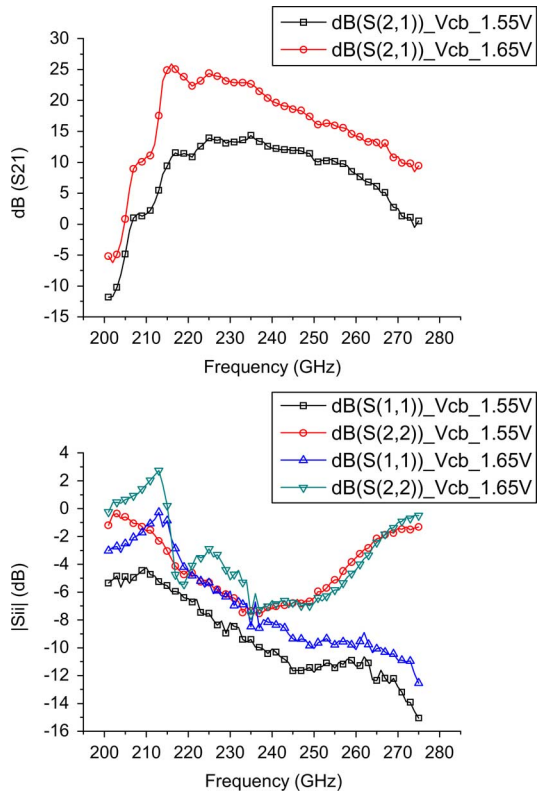

Fig. 8. Measured results of the 265-GHz LNA with different current density: 29 mA · 2 V($V_{\rm cb}$: 1.65 V) and 14 mA · 2 V($V_{\rm cb}$: 1.55 V), run1 .

IV. Simulation and Measurement Results

We measured receiver and sub-circuit chips, which were fabricated in three subsequent technology runs: run1, run2, and run3.

A. CB LNA in Run1

In run1, 0.25-μm SG25 H1 (DotFive) technology is utilized. Fig. 7 shows a chip photograph of the fabricated CB LNA in run1. The chip size is 0.42 · 0.46 mm^2, ground–signal–ground (GSG) input and output bond pads with 80-μm-pitch length are utilized for on-wafer measurement. Metal1 shielding is adopted for the pad design in order to prevent substrate loss and obtain a high-Q pad capacitance. On the left and right side are the input and output bond pads. On the top are the VCC and $V_{\rm cb}$ pads. Channel stop implant was blocked at critical places such as input, output pad, transmission lines, and long inter connects, in order to reduce the ohmic loss. Large areas of decoupling MIM capacitors are also included in the chip between the supply and ground.

For a frequency as high as 245 GHz, frequency shifts can occur for LNAs even if minor parasitics, such as pieces of short interconnects, the terminal connections, and parasitic bottom capacitor of the MIM capacitor, are introduced [13]. Thus, in order to give some frequency margin for measurement, in run1, two LNAs peaking at 245 and 265 GHz were designed. The two LNAs are both input and output matched to 50 Ω. They can achieve 13- and 10-dB gain, 12- and 14-dB NF, respectively, at the designed frequency. S-parameter and noise simulation results of the two LNAs could be referred in [10]. Unconditional stability of the LNA is verified from dc to 300 GHz.

Fig. 8 shows the measurement result of the 265-GHz LNA. During the measurement with the original bias points in simulation, the LNA is unstable, and by reducing the bias voltage at the base terminal $V_{\rm cb}$ from 1.8 to 1.55 V, the LNA becomes stable again. In order to give complete information, measurement results of two typical bias points are given. The LNA with $V_{\rm cb}$ of 1.65 V is not stable, with $S22$ at 212 GHz above 0. It has a power dissipation of 29 mA · 2 V. The LNA with $V_{\rm cb}$ of 1.55 V is stable while exhibiting a power dissipation of 14 mA · 2 V. For the latter, the peak frequency shifts to 235 GHz. It has 12-dB gain at 245 GHz, and a 3-dB bandwidth of 26 GHz.

As mentioned in Section III-A, a parasitic inductance is utilized in this study to boost the gain of the LNA, and due to the introduction of the inductance, a negative resistance is introduced at the input of the CB LNA stage. By decreasing the base terminal bias voltage, the negative resistance decreases, gain of the LNA is reduced, and stability of the LNA is improved. This explains well the phenomenon that the LNA becomes stable when base bias voltage $V_{\rm cb}$ reduces from 1.65 to 1.55 V in Fig. 8.

In order to further verify the explanation, in simulation, an inductance of 4 pH is inserted between the base terminal and bypass capacitors (ac ground) for the 265-GHz LNA, and biased with the measured bias voltage value. S-parameter simulation results of the LNA including the parasitic inductance is shown in Fig. 9. In comparison, the measurement result is also plotted. The peak frequency is shifted to around 245 GHz due to the parasitic inductance, and the LNA could achieve higher gain even with lower collector current density. The simulation confirms the measurement result. Unconditional stability is verified from

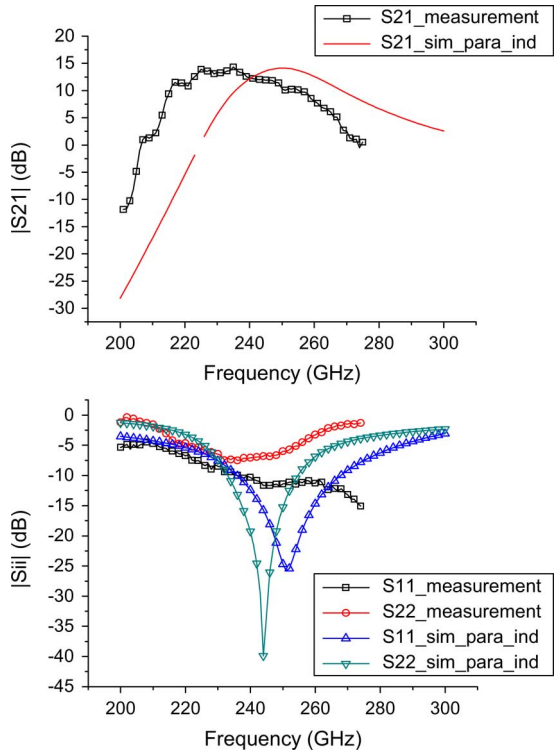

Fig. 9. Simulation results (16 mA · 2 V, $Vcb = 1.55$ V) compared with measurement results (14 mA · 2 V, $Vcb = 1.55$ V) when the base inductance is included, run1.

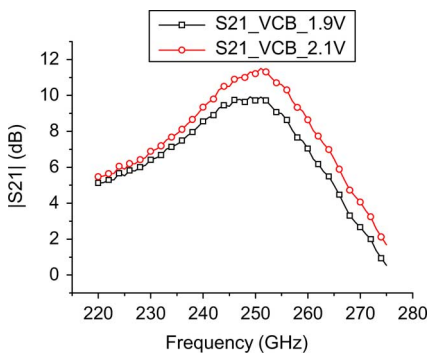

Fig. 10. $S21$ sensitivity versus base bias $V_{\rm cb}$, run3.

2 to 300 GHz. Nevertheless, between dc and 2-GHz conditional stability is verified for specific frequency range.

Furthermore, with a reduced bias voltage value, taking advantage of the parasitic inductance, the LNA can have even smaller simulated NF, which is only 11 dB at 245 GHz. NF simulation results are given in [10].

In run1, the base of the LNA is biased from a resistor ladder rendering the LNA performance very sensitive to $V_{\rm cb}$. As mentioned in Section III-A, the more accurate diode-connected transistor bias circuit is utilized in run3 to decrease the sensitivity of the gain of LNA. In Fig. 8, $S21$ of the LNA at 245 GHz changes from 12 to 18.5 dB when $V_{\rm cb}$ changes from 1.55 to 1.65 V. Fig. 10 presents LNA sensitivity versus base bias $V_{\rm cb}$ in run3 in order to give a comparison. In run3, $S21$ increases from 9.5 to 11 dB when $V_{\rm CB}$ changes from 1.9 to 2.1 V. Therefore, the LNA becomes much less sensitive to $V_{\rm CB}$ with the diode-connected bias circuit.

TABLE II
PERFORMANCE COMPARISON OF THREE LNAs

	power	Gain	3dB bandwidth
[3]	144 mW	15dB@210GHz	25 GHz
Run1	28 mW	12dB@245GHz	26 GHz
Run3	44 mW	11dB@245 GHz	24 GHz

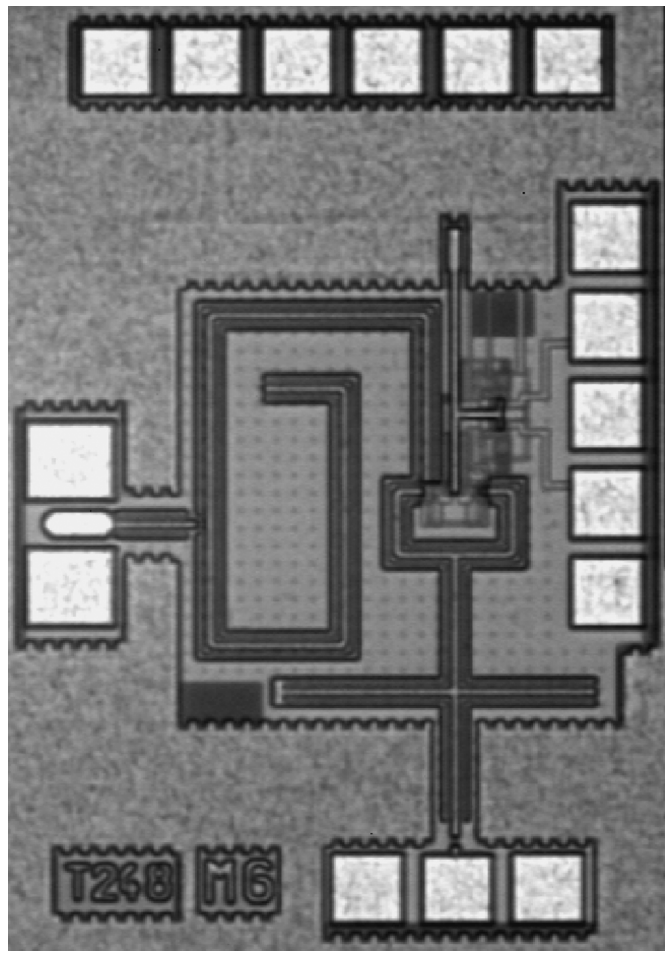

Fig. 11. Chip photograph of the fourth transconductance SHM, run2.

Due to the limitation of the measurement equipment, the NF is not measured. Table II shows a performance comparison of the 220-GHz LNA in [3] with an LNA of this study. Both the CB LNA in run1 and run3 are included in the table to give a comparison. With comparable gain and bandwidth performance, the LNA in run1 dissipates only 1/5 the power of the LNA in [3], and the LNA in run3 consumes only less than 1/3 the power of the LNA in [3]. The four-stage CB LNA therefore features high gain and wide bandwidth while dissipating little power.

The same topology of CB LNA as in run1 was designed and fabricated. However, according to measurement results, this LNA does not work properly and achieves a gain of merely -5 dB in run2. This is because $f_{\rm max}$ of transistors in IHP GmbH's SG13S technology is 300 GHz, which is close to the RF operating frequency 245 GHz, and hence, positive power gain is difficult to achieve.

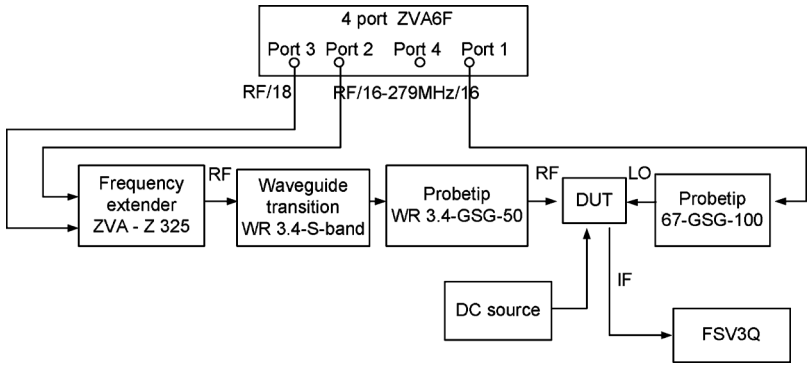

Fig. 12. Measurement setup.

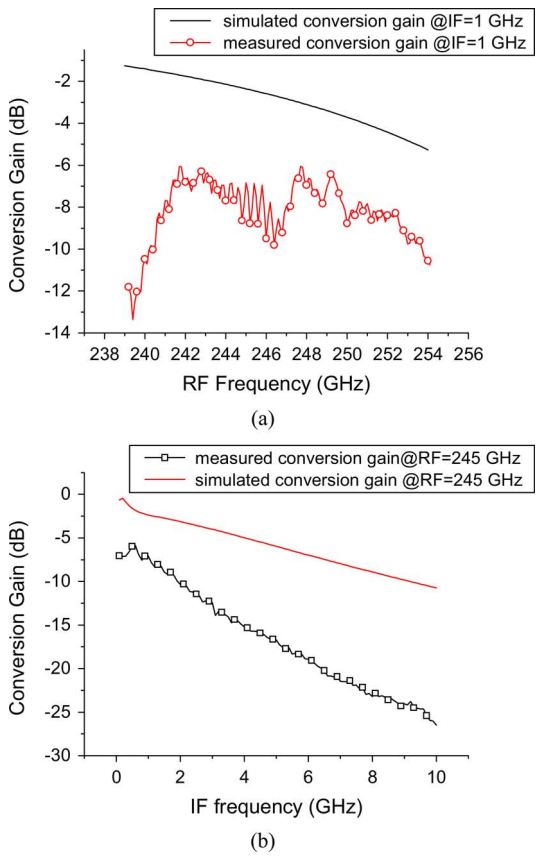

Fig. 13. Measurement and simulation results of the mixer, run2.

TABLE III
PERFORMANCE COMPARISON OF SHMs

	RF/ft/fmax	Order subharmonic	Conv. Gain dB	NF (sim) dB
[6] (meas)	77/80/-	2nd	0.7	23
Run2 (meas)	245/250/300	4th	-7	39
Run3 (meas)	245/300/500	4th	-5	33
Run3 (sim)	245/300/500	2nd	14	25

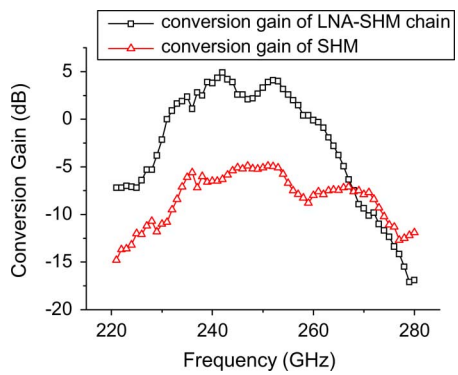

Fig. 14. Conversion gain of SHM, LNA-SHM chain.

B. CB LNA and Fourth SHM in Run2

Both the four-stage CB LNA and fourth transconductance SHM are designed and fabricated in run2. In run2, IHP 0.13-μm SG13S technology was utilized.

Fig. 11 shows a chip photograph of the fourth transconductance SHM in run2. Chip size is $1 \cdot 0.75$ mm^2. On the left are GSG RF input pads, and on the right are the differential ground–signal–ground–signal–ground (GSGSG) IF output pads. At the bottom, the 60-GHz LO input pads are located. On the top, the dc pads are placed [13].

Fig. 12 shows the measurement setup for the fourth transconductance SHM. Four-port network analyzer ZVA6F provides RF signals RF/18 and (RF/16–279 MHz/16) to frequency extender Z325. A 245-GHz RF signal is obtained by the RF signal multiplications in Z325. A 245-GHz RF signal is supplied to the device-under-test (DUT) through the waveguide transition S-band WR 3.4-S-band and probe tip WR 3.4-GSG-50. A 61-GHz LO signal is supplied by ZVA6F directly to the DUT. An IF signal is displayed on spectrum analyzer FSV3Q.

Measurement and simulation results for the subharmonic mixer are shown in Fig. 13. The mixer was measured with LO power of 8 dBm for saturation. Fig. 13(a) shows the conversion gain of the mixer when the IF is fixed at 1 GHz. It indicates that the conversion gain is -7 dB when the RF frequency is 245 GHz with a 3-dB conversion gain of -9- $\sim$ -6-dB bandwidth from 240.5 to 252.7 GHz. The simulated gain of the buffer is 6 dB, so the conversion gain of the mixer core alone is from -16 to -13 dB in the frequency range from 239 to 253 GHz. Fig. 13(b) shows the IF frequency response. The conversion gain decreases when the IF frequency increases. Gain drops when the IF frequency decreases due to the dc blocking capacitors between the mixer and buffer stage. In Fig. 13(a) and (b), the differences between the simulated and measured conversion gain is about -5 dB at an operating frequency

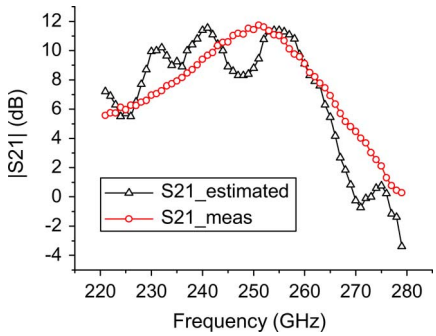

Fig. 15. Estimated $S21$ of the LNA and $S21$ of the standalone LNA, run3.

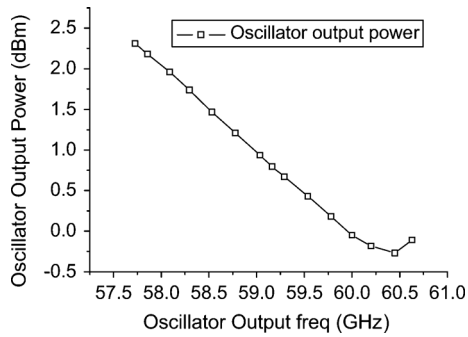

Fig. 16. Oscillator output power versus oscillator output frequency, run3.

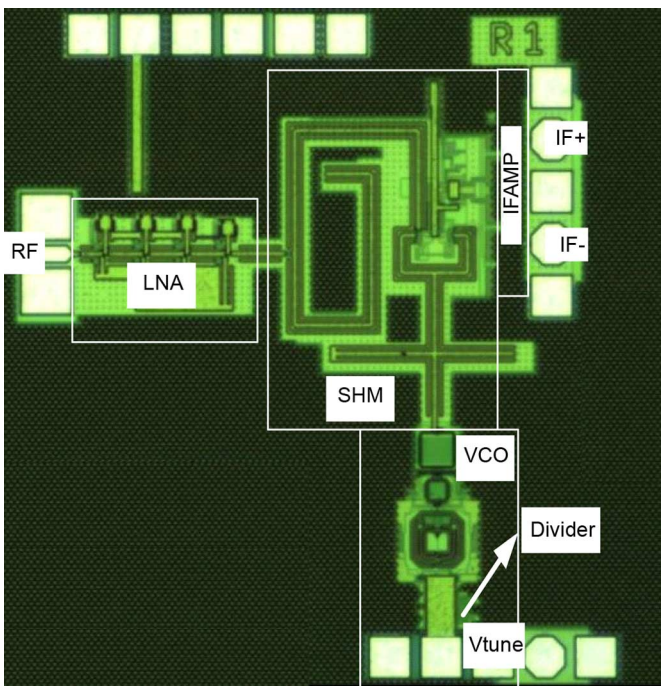

Fig. 17. Chip photograph of the receiver, run3.

of 245 GHz, and this could be due to the inaccuracies of the transistor models or the EM simulation of the passives.

The simulated output 1-dB compression point is -9.1 dBm. The simulated NF is 39 dB at 245 GHz. Table III gives a performance comparison between the second transconductance SHM and the fourth transconductance SHM of different technologies. For both the second SHM [6] and fourth SHM in run2, the RF frequency is very close to f_T of the technology. Comparing the two SHMs, conversion gain of the fourth SHM is lower than that of the second SHM, and the NF is relatively higher. In run3, a

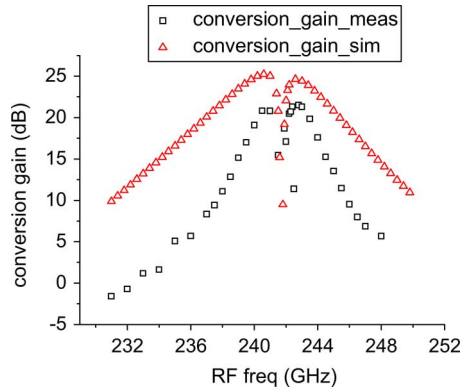

Fig. 18. Conversion gain of the receiver versus IF frequency.

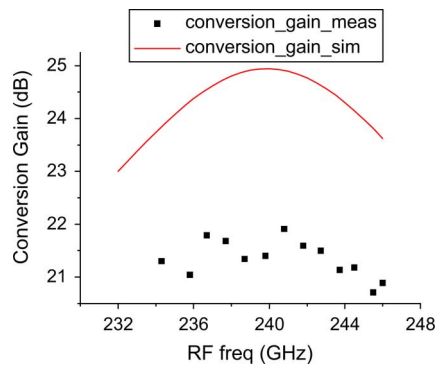

Fig. 19. Conversion gain of the receiver versus RF frequency with fixed IF frequency of 1 GHz.

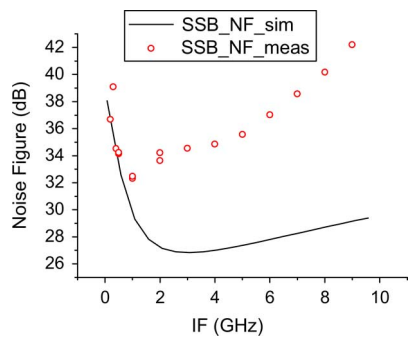

Fig. 20. SSB NF of the receiver versus IF frequency.

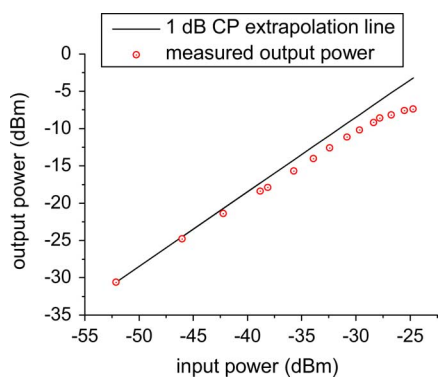

Fig. 21. Output power versus input power sweep.

fourth SHM is designed and measured, while a second SHM is designed, but not yet measured. Both the measurement results of fourth SHM and simulation results of second SHM in run3 are included in Table III for comparison. Comparing the

TABLE IV
COMPARISON OF STATE-OF-THE-ART

	RF (GHz)	ft/fmax (GHz)	Integration level	Local Oscillator (GHz)	Conv. Gain (dB)	Power Dissipation (mW)	NF (dB)	Technology
[16]	220	-	Antenna, LNA, Mixer	55	3.5	110	7.4	0.1 μm mHEMT
[17]	220	-	Ant., LNA, Mixer, LO-chain	109	2	-	8.4	0.1 μm mHEMT
[18]	220	280/435	LNA, Mixer	110	16	216	18	0.13 μm SiGe HBT
Run3	245	300/500	LNA, 4th SHM, IFAMP, VCO	61	21	358/158 (with/ without VCO)	32	0.13 μm SiGe HBT
Run3 (sim)	245	300/500	LNA, 2nd SHM	122	21	145	19	0.13 μm SiGe HBT

fourth SHM with simulation results of the second SHM in the same technology run3, a similar conclusion such as above can be drawn. Future work will be carried out using a second transconductance SHM and a passive SHM to achieve lower NF.

C. Integrated Receiver in Run3

In run3, IHP GmbH 0.13-μm SG13G2 technology is utilized. Besides a standalone 60-GHz VCO, a CB LNA, a fourth transconductance SHM and an LNA-SHM chain, an integrated receiver comprised of a CB LNA, a SHM, and a 60-GHz VCO was designed and fabricated in run3.

The CB LNA, SHM, LNA-SHM chain, and VCO were designed as separate components. Conversion gain of both the SHM and LNA-SHM chain are measured with external 60-GHz LO sources. Measurement setup of the receiver and SHM is illustrated in Fig. 12. Fig. 14 presents the conversion gain of the SHM and LNA-SHM chain when the IF frequency is fixed at 1 GHz and RF and LO frequencies sweep simultaneously with an LO power of 8 dBm for saturation. Accordingly, $S21$ of the CB LNA could be estimated by subtracting the conversion gain of the SHM from the conversion gain of the LNA-SHM chain. Fig. 15 presents both the estimated $S21$ of the CB LNA and $S21$ of the standalone CB LNA from measurement. In Fig. 15, there are some differences between the estimated and measurement $S21$ results in the frequency range of 220–240 GHz. This may be due to the small modification in the output matching of the LNA when it is connected to the fourth SHM. However, the rough values of the two are similar. $S21$ of the CB LNA has a 3-dB bandwidth extending from 237 to 261 GHz. A gain of 11 dB is achieved at 243 GHz, and the simulated NF is 12 dB. Fig. 16 shows the measurement results of the VCO.

In Fig. 16, when the VCO tuning voltage $V\mathrm{tune}$ changes from 0 to 3 V, the oscillating frequency changes from 57.7 to 60.6 GHz. The VCO has a peak output power of 2.3 dBm at 57.7 GHz, and a minimum output power of -0.2 dBm at 60.4 GHz.

The chip photograph of the complete integrated receiver is shown in Fig. 17. The chip size is 1.1×1.3 mm^2. Large areas of decoupling MIM capacitors are included in the chip between the supply and the ground.

The receiver was measured applying 2-V LNA supply voltage with a current of 22 mA, a 3-V SHM supply voltage with current of 16 mA, a 1.3-V supply voltage of IFAMP with current of 13 mA, and a 3.3-V supply voltage of the VCO with a current of 63 mA. The total chip dissipates 358 mW.

TABLE V
CIRCUIT PERFORMANCE VERSUS TECHNOLOGY

	Technology/ft/fmax	Gain/Conv. Gain (dB)
CB LNA	Run1/300/500	12 dB
CB LNA	Run2/250/300	-6 dB
CB LNA	Run3/300/500	11 dB
Transconductance SHM	Run2/250/300	-7 dB
Transconductance SHM	Run3/300/500	-5 dB

Fig. 18 shows the single-ended conversion gain of the receiver with fixed VCO tuning voltage $V\mathrm{tune}$ of 2 V with corresponding VCO frequency at 60.4 GHz, when the input RF frequency is swept. The receiver achieves 21-dB peak-conversion gain at IF frequency of 1 GHz. Measurement results agree with the simulation results. The conversion gain decreases when the IF frequency decreases due to the dc blocking capacitor (1 pF) between the fourth subharmonic mixer and the IF buffer amplifier. The 3-dB bandwidth at the upper sideband reaches from 241.8 to 243.9 GHz, with the IF 3-dB bandwidth extending from 0.1 to 2.2 GHz. 3-dB RF bandwidth in the lower sideband extends from 239.7 to 241.3 GHz in the mirror, with the IF 3-dB bandwidth extending from 0.4 to 2 GHz. 1-dB compression point is at -37 dBm with IF frequency of 1 GHz and $V\mathrm{tune}$ of 2 V. IFAMP contributes around 16-dB gain in the receiver, which is calculated from the difference between the conversion gain of the subharmonic receiver (21 dB) and that of the standalone LNA-mixer chain (5 dB).

Fig. 19 presents the conversion gain of the receiver versus RF frequency with tuning voltage from 0 to 3 V and fixed IF frequency of 1 GHz. The input RF frequency is swept from 234 to 246 GHz while keeping the IF frequency constant. A tuning bandwidth of 12 GHz is achieved, and in the whole frequency range, the conversion gain is nearly flat.

With an LO frequency of 60.4 GHz, IF frequency at 1 GHz, corresponding RF frequency of 242.7 GHz, a -121-dBm/Hz output noise power is obtained. According to spectrum analyzer specifications, a 95% confidence level is achieved within 0.28-dB deviation. With 21-dB conversion gain, this corresponds to a 32-dB single-sideband (SSB) NF, which exceeds the simulated SSB NF of the receiver 28 by 4 dB. This is probably due to the inaccuracy in modeling. In simulation, the

TABLE VI
PERFORMANCE COMPARISON UPON DIFFERENT RECEIVERS

	CB LNA, 4th transconductance SHM, IFAMP	CB LNA, 2nd transconductance SHM	CB LNA, 2nd passive SHM, IFAMP	2nd passive SHM, IFAMP
Conversion gain (dB)	21 (meas)	25.57	24.1	12.5
Output 1 dB compression point (dBm)	-16 (meas)	3.65	0.28	0
Noise figure (dB)	33 (meas)	19.1	15.8	20.7

NF of the LNA alone is 11.7 dB at 243 GHz, according to Friis equation, the relatively high NF of the fourth SHM leads to the high overall NF 32 dB.

Fig. 20 presents the measured and simulated SSB NF of the receiver versus IF frequency. SSB NF increases when IF decrease toward dc due to the reduction of the conversion gain. Measurement results agree well with the simulation results.

Fig. 21 presents measurement results of the output power versus input power sweep. A 1-dB compression point is at -37 dBm extrapolated from the power sweep.

Table IV gives a performance comparison between the receiver of this study and state-of-the-art. Integrated with a 60-GHz VCO, the subharmonic receiver in this study has a higher integration level compared with the state-of-the-art. Although the fourth SHM in this study leads to high overall NF (32 dB) in the chain, simulation results shows that receiver with a second SHM can achieve unproven NF (19 dB) with smaller power dissipation (145 mW).

V. DISCUSSION

A. f_T, $f_{\max}$ Upon Linear and Nonlinear Circuits

In each technology run, standalone CB LNA and SHM circuit blocks with the same topologies were designed and compared. Table V gives a summary on the comparison of circuit blocks in the three technology runs.

From Table V, in three different technology runs, f_T is similar, about 300 GHz for each, but $f_{\max}$ varies a lot. $f_{\max}$ of Run1 and run3 (500 GHz) is nearly twice that of run2 (300 GHz).

In Table V, we come to the conclusion that for a linear circuit block such as the LNA, $f_{\max}$ is the main limitation factor for increasing RF operating frequency. Obviously, it is difficult to amplify RF signal power working close or above $f_{\max}$. In run1 and run3, $f_{\max}$ of transistors are two times the RF frequency of 245 GHz, and hence, the LNA shows a nice gain performance (12 dB) at 245 GHz. While for nonlinear circuits like the frequency translation circuit block SHM, $f_{\max}$ plays a much less important role in the performance. In both run 2 and run 3, SHMs achieve a conversion gain around -5 dB. According to Table III, they also have similar noise performance, although in run3 the transistors have twice the $f_{\max}$ of the transistors in run2. Signal power amplification could be obtained through frequency translation.

As the RF operating frequency increases, due to the limitation of $f_{\max}$, the gain of the LNA decreases and the LNA might be unable to suppress noises from subsequent stages. In this case, a receiver without an LNA, which directly converts RF signals into IF signals, is possible to obtain better performance, as shown in [7].

B. Systematic Design of a 245-GHz Receiver Topology

As mentioned in Section I, besides the fourth transconductance SHM, there exist other mixer topologies like passive SHM and active ones. By combining the CB LNA with different SHMs, receivers with different features could be achieved. In this study, although measurement results from various other receiver topologies are not ready yet, some systematic simulation results are given and discussed.

Different receivers, e.g., a receiver comprising of the CB LNA and a second transconductance SHM chain, a receiver comprised of the CB LNA, a second passive SHM, and an IFAMP chain, are simulated and compared. As mentioned in Section V-A, if the LNA could not provide enough gain to suppress noise, it is possible that a receiver without an LNA that directly converts RF signals into IF signals might achieve better performance. Thus, a receiver comprised of the second transconductance SHM-IFAMP chain is also simulated.

In summary, Table VI gives a comparison between the different receiver topologies. At 245 GHz, the receiver comprised of the CB LNA and second transconductance SHM, and the receiver comprised of the CB LNA, second passive SHM, and IFAMP have better gain and noise performance than a receiver comprising of the second passive SHM and IFAMP. The LNA has enough gain to suppress noise from subsequent stages. The receiver comprised of the CB LNA, second passive SHM, and IFAMP has the best noise performance. Although Table VI is unproven by measurement results, it gives some guidelines for system design of the receiver at 245 GHz.

VI. CONCLUSION

A four-stage CB 245-GHz LNA and a fourth subharmonic 245-GHz transconductance mixer have been designed and measured. The LNA has 12-dB gain, 25-GHz 3-dB bandwidth, and a power dissipation of 28 mW, and the mixer has -7-dB conversion gain. The LNA achieves high gain and wide bandwidth while exhibiting small power consumption. A 245-GHz subharmonic receiver comprised of the CB LNA, the fourth transconductance SHM, IF amplifier, and a 60-GHz VCO was presented. The receiver reaches 21-dB gain at 243 GHz with a tuning range of 12 GHz and an NF of 32 dB. A 19-dB NF is feasible in case of a second transconductance SHM.

ACKNOWLEDGMENT

The authors are thankful for the pilot line staff, IHP GmbH, Frankfurt (Oder), Germany, for excellent fabrication of the chip.

REFERENCES

[1] K. Schmalz, W. Winkler, J. Borngräber, W. Debski, B. Heinemann, and J. C. Scheytt, "A subharmonic receiver in SiGe technology for 122 GHz sensor applications," *IEEE J. Solid-State Circuits*, vol. 45, no. 9, pp. 1644–1656, Sep. 2010.

[2] L. Persson, M. Sjoholm, G. Hong, M. Andersson, and S. Svanberg, "Tunable diode laser spectroscopy for gas detection inside scattering media," in *Eur. Lasers Electro-Opt. Conf.*, 2005, p. 646.

[3] E. Öjefors, B. Heinemann, and U. R. Pfeiffer, "A 220 GHz subharmonic receiver frond end in a SiGe HBT technology," in *IEEE RFIC Symp. Dig.*, 2011, pp. 1–4.

[4] Y. Sun, J. Borngraber, F. Herzel, and W. Winkler, "A fully integrated 60 GHz LNA in SiGe:C BICMOS technology," in *IEEE BCTM Symp. Dig.*, 2005, pp. 14–17.

[5] W. Winkler, W. Debski, B. Heinemann, F. Korndorfer, H. Rücker, K. Schmalz, J. C. Scheytt, and B. Tillack, "122 GHz low-noise-amplifier in SiGe technology," in *IEEE ESSCIRC Symp. Dig.*, 2009, pp. 316–319.

[6] J.-J. Hung, T. M. Hancock, and G. M. Rebeiz, "A 77 GHz SiGe subharmonic balanced mixer," *IEEE J. Solid-State Circuits*, vol. 40, no. 11, pp. 2167–2173, Nov. 2005.

[7] E. Öjefors, B. Heinemann, and U. R. Pfeiffer, "A 650 GHz SiGe receiver front-end for terahertz imaging arrays," in *IEEE Int. Solid-State Circuits Conf. Symp. Dig.*, 2010, pp. 430–431.

[8] M. W. Chapman and S. Raman, "A 60-GHz uniplanar MMIC 4× subharmonic mixer," in *IEEE MTT-S Int. Microw. Symp. Dig.*, 2001, vol. 1, pp. 95–98.

[9] H. Rücker, B. Heinemann, and A. Fox, "Half-terahertz SiGe BICMOS technology," in *IEEE BCTM Symp. Dig.*, 2012, pp. 133–136.

[10] Y. Mao, K. Schmalz, J. Borngräber, and J. C. Scheytt, "A 245 GHz CB LNA in SiGe," in *IEEE EuMIC Symp. Dig.*, 2011, pp. 224–227.

[11] R. G. Paul, J. H. Paul, H. L. Stephen, and G. M. Robert, *Analysis and Design of Analog Integrated Circuits*, 4th ed. New York: Wiley, 2001, pp. 34–36.

[12] Y. Mao, K. Schmalz, J. Borngraber, and J. C. Scheytt, "A 245 GHz CB LNA and SHM mixer in SiGe technology," in *IEEE Silicon Monolithic Integr. Circuits RF Syst. Top. Meeting*, 2012, pp. 5–8.

[13] Y. Mao, K. Schmalz, J. Borngräber, and J. C. Scheytt, "Comparison of 122 GHz LNAs in SiGe with different transmission line topologies," in *IEEE MTT-S Microw. Workshop*, 2011, pp. 152–155, Ser. Millimet. Wave Integration Technol..

[14] S. Decoutere, S. Van Huylenbroeck, B. Heinemann, A. Fox, P. Chevalier, A. Chantre, T. F. Meister, K. Aufinger, and M. Schröter, "Advanced process modules and architecture," in *Proc. BCTM*, Oct. 2009, pp. 9–16.

[15] H. Rücker, B. Heinemann, W. Winkler, R. Barth, J. Borngräber, J. Drews, G. Fischer, A. Fox, T. Grabolla, U. Haak, D. Knoll, F. Korndörfer, A. Mai, S. Marschmeyer, P. Schley, D. Schmidt, J. Schmidt, K. Schulz, B. Tillack, D. Wolansky, and Y. Yamamoto, "A 0.13 μm SiGe BICMOS technology featuring $fT/f\max$ of 240/330 GHz and gate delays below 3 ps," in *Proc. BCTM Conf.*, 2009, pp. 166–169.

[16] M. Abbasi, S. E. Gunnarsson, N. Wadefalk, R. Kozhuharov, J. Svedin, S. Cherednichenko, I. Angelov, I. Kallfass, A. Leuther, and H. Zirath, "Single-chip 220-GHz active heterodyne receiver and transmitter MMICs with on-chip integrated antenna," *IEEE Trans. Microw. Theory Tech.*, vol. 59, no. 2, pp. 466–478, Feb. 2011.

[17] S. E. Gunnarsson, N. Wadefalk, J. Svedin, S. Cherednichenko, I. Angelov, H. Zirath, I. Kallfass, and A. Leuther, "A 220 GHz single-chip receiver MMIC with integrated antenna," *IEEE Microw. Wireless Compon. Lett.*, vol. 18, no. 4, pp. 284–286, Apr. 2008.

[18] E. Öjefors, B. Heinemann, and U. R. Pfeiffer, "Subharmonic 220- and 320-GHz SiGe HBT receiver front-ends," *IEEE Trans. Microw. Theory Tech.*, vol. 60, no. 5, pp. 1397–1404, May 2012.

Yanfei Mao received the Master's degree in microelectronics from the Technical University of Delft (TU Delft), Delft, The Netherlands, in 2009.

She is currently with IHP GmbH, Frankfurt (Oder), Germany, where he has been involved in the field of RF circuit design. Since joining IHP GmbH, she has authored three papers concerning RF circuit design. Her research interest is the 245-GHz receiver in SiGe BiCMOS technology for sensor applications.

Klaus Schmalz received the Ph.D. degree in physics from the Humbolt University of Berlin, Berlin, Germany, in 1978.

He is currently with IHP GmbH, Frankfurt (Oder), Germany. He has been involved in the field of silicon semiconductor technologies and research and possesses expertise in the area of thermally induced defects and characterization of Si/SiGe structures. After training in RF circuit design at the University of California at Los Angeles (UCLA), from 1998 to 1999, he changed his scientific focus to RF analog circuit design. He has authored or coauthored over 100 papers. His research interest is the design of SiGe BiCMOS analog circuits for wireless communication with emphasis on RF frontends for different standards and millimeter-wave circuits for sensor applications.

Johannes Borngräber received the Diploma of mathematics degree from Humboldt University, Berlin, Germany, in 1981.

Since 1994, he has been with the Department of Circuit Design, IHP GmbH, Frankfurt (Oder), Germany. He is currently especially interested in NF and phase-noise measurement techniques in the millimeter-wave range.

John Christoph Scheytt received the Diploma degree (M.S.) and Ph.D. degree with highest honors) from Ruhr-University Bochum, Germany, in 1996 and 2000, respectively.

In 2000, he cofounded advICo Microelectronics GmbH, a German integrated circuit (IC) design house. For six years, he was the Chief Executive Officer (CEO) with advICo Microelectronics GmbH, where he was responsible for various projects in the area of wireless and fiber-optic IC design. From 2006 to 2012, he was with Head of the Circuit Design Department (a group of about 30 researchers involved with high-frequency and broadband IC design), IHP GmbH. In 2012, he became a Professor of circuit design with the University of Paderborn, Paderborn, Germany. He has authored or coauthored over 80 papers. He holds 12 patents. His research interests include RF integrated circuit (RFIC) and broadband IC design, phase-locked loop (PLL) techniques, and design with SiGe BiCMOS technologies.